

Open Data from LIGO, Virgo, and KAGRA through the First Part of the Fourth Observing Run

THE LIGO SCIENTIFIC COLLABORATION, THE VIRGO COLLABORATION, AND THE KAGRA COLLABORATION

ABSTRACT

LIGO, Virgo, and KAGRA form a network of gravitational-wave observatories. Data and analysis results from this network are made publicly available through the Gravitational Wave Open Science Center. This paper describes open data from this network, including the addition of data from the first part of the fourth observing run (O4a) and selected periods from the preceding engineering run, collected from May 2023 to January 2024. The public data set includes calibrated strain time series for each instrument, data from additional channels used for noise subtraction and detector characterization, and analysis data products from version 4.0 of the Gravitational-Wave Transient Catalog.

1. INTRODUCTION

The Laser Interferometer Gravitational-Wave Observatory (LIGO; [Aasi et al. 2015](#)), Virgo ([Acernese et al. 2015](#)), KAGRA ([Akutsu et al. 2021a](#)) and GEO 600 ([Luck et al. 2010](#); [Affeldt et al. 2014](#); [Dooley et al. 2016](#)) are observing the gravitational-wave (GW) Universe with unprecedented sensitivity ([Abac et al. 2025a](#)). Data from these observatories are shared and jointly analyzed as described in a Memorandum of Agreement ([LIGO, Virgo, and KAGRA 2019](#)), so that the instruments form a global network. The instruments operate in a series of observing runs, with breaks between observing periods for instrument upgrades and detector commissioning ([Abbott et al. 2020a](#); [Capote et al. 2025](#)). Following a proprietary period for work by the LIGO–Virgo–KAGRA Collaboration (LVK), data from each observing run are publicly released via the Gravitational Wave Open Science Center (GWOSC) for use by the entire scientific community.¹ The schedule of data releases for LIGO is maintained in the LIGO Data Management Plan ([LIGO Laboratory 2025](#)).

Data from previous observing runs have been released with a history going back more than a decade, starting with data from initial LIGO released in 2014 ([Vallisneri et al. 2015](#)). Data from the advanced-detector era are organized into an ongoing series of observing runs, beginning with data from the first observing run (O1) and second observing run (O2; [Abbott et al. 2021a](#)), and continuing with data released from the third observing run (O3; [Abbott et al. 2023a](#)).

The fourth observing run is divided into several segments, with the first segment (O4a) spanning time from May 24, 2023 to January 16, 2024. This paper describes the publicly available data from the LVK with an emphasis on the new O4a public data release. At the time of this writing, as described in Subsection 2.1, this data release includes data from LIGO only.

Public data include time series strain data from the instruments, additional time series channels describing the instrument state, and segment information describing data quality of each instrument. In addition, the full set of events known as the Gravitational-Wave Transient Catalog (GWTC) identified by the LVK is publicly available. The O4a data release also includes a number of analysis results from the fourth version of the Gravitational-Wave Transient Catalog (GWTC-4.0, [Abac et al. 2025b](#)), including an electronic version of the catalog that can be browsed online and queried through a Representational State Transfer Application Programming Interface (REST API). This paper is included in a suite of papers describing GWTC-4.0 ([Abac et al. 2025a](#)), and is best understood in the context of the related papers.

In Section 2 we discuss the primary data products from GW observatories and the epochs of data taking known as observing runs. In Section 3 we explain the basics of calibration of interferometer strain data. Section 4 outlines some non-astrophysical noise sources that impact GW data analysis and noise mitigations. In Section 5 we describe the details for the strain data available on GWOSC and alternative services. Section 6 discusses additional instrumental monitoring channels used for noise subtraction and production of data-quality flags that are now also distributed by GWOSC. Finally, the GWOSC Event Portal that provides electronic catalogs of detected GW transients is described in Section 7.

2. DATA SET OVERVIEW

2.1. Observing Time

The instruments operate in a series of observing runs described in [Abac et al. \(2025a\)](#), with the following dates:

- O1: 12 September 2015 0:00 UTC (GPS 1126051217) to 19 January 2016 16:00 UTC (GPS 1137254417)
- O2: 30 November 2016 16:00 UTC (GPS 1164556817) to 25 August 2017 22:00 UTC (GPS 1187733618)

¹ GWOSC Home Page, <https://gwosc.org>

- O3: 1 April 2019 15:00 UTC (GPS 1238166018) to 27 March 2020 17:00 UTC (GPS 1269363618)
- O4a: 24 May 2023 15:00 UTC (GPS 1368975618) to 16 January 2024 16:00 UTC (GPS 1389456018)

The O4a data release also includes some additional data from the preceding engineering run (see Section 5.3). Some observational data are also available from other times studied in targeted LVK publications, including data from the GEO 600 (Dooley et al. 2016) and KAGRA (Akutsu et al. 2021a) detectors, as described in LIGO Scientific Collaboration, Virgo Collaboration and KAGRA Collaboration (2017, 2022, 2024).

The observatories do not record astrophysical data at all times. Many types of phenomena can interrupt data taking, including instrument maintenance and detector improvements, seismic activity, power outages, and instrument lock-loss for other reasons. A comparison of the total amount of observing time for each run is shown in Table 1. The amount of calendar time for each observing run is shown at the top of each table section (e.g., O4a spanned 237 calendar days). The O3 runs includes observing time from both O3a and O3b, as well as a commissioning break with no observing time.

During O4a, Virgo was not observing due to commissioning activities. KAGRA and GEO 600 data were less sensitive than the other observatories, and so were not used for most analyses. Therefore, only data from LIGO are included in this data release. The total coincident time with both LIGO Hanford Observatory (LHO) and LIGO Livingston Observatory (LLO) observing simultaneously during O4a was 126.5 days. The table shows similar statistics for each of O1, O2, and O3, with additional information on past data releases available in Abbott et al. (2021a) and Abbott et al. (2023a).

2.2. Time-series Data

The primary data product from a GW observatory is the calibrated strain data, often called $h(t)$. The strain data are recorded as a time series, so that each time sample records one measurement of the fractional difference in lengths in the interferometer arms, $\Delta L/L$. The LIGO, Virgo, and KAGRA observatories typically use a sampling rate of 16384 samples per second, corresponding to a data rate of ~ 4 TB per year per instrument for the strain data. This is a small fraction of the total data rate of several PB per year, which includes hundreds of thousands of diagnostic channels to monitor the state of the instrument and the local environment.

For current instruments, the strain time series consists primarily of instrumental noise at most times (Abbott et al. 2020b). The noise levels in the instruments fluctuate over time, so that the sensitivities of the instruments vary from moment to moment. One long-used figure of merit for the instrument sensitivity is the binary neutron star (BNS) inspiral range (Finn & Chernoff 1993; Chen et al. 2021), which is briefly summarized in Abac et al. (2025a), and gives

Table 1. The amount of observing time in days and the corresponding fraction of the total run time for each detector (IFO) combination. The amount of calendar time for each observing run is shown at the top of each table section.

IFO Combination	Observing Time	Fraction
O1: 129.7 d		
LHO	27.7 d	21.4 %
LLO	16.8 d	13.0 %
LHO, LLO	49.0 d	37.8 %
O2: 268.3 d		
LHO	37.8 d	14.1 %
LLO	33.5 d	12.5 %
Virgo	1.7 d	0.6 %
LHO, LLO	103.0 d	38.4 %
LHO, Virgo	1.7 d	0.6 %
LLO, Virgo	2.2 d	0.8 %
LHO, LLO, Virgo	15.3 d	5.7 %
O3a: 183.0 d		
LHO	5.6 d	3.1 %
LLO	6.3 d	3.4 %
Virgo	15.7 d	8.6 %
LHO, LLO	25.9 d	14.2 %
LHO, Virgo	17.5 d	9.5 %
LLO, Virgo	25.3 d	13.8 %
LHO, LLO, Virgo	80.8 d	44.2 %
O3b: 147.1 d		
LHO	4.5 d	3.1 %
LLO	3.4 d	2.3 %
Virgo	9.3 d	6.3 %
LHO, LLO	22.9 d	15.6 %
LHO, Virgo	14.5 d	9.8 %
LLO, Virgo	13.8 d	9.4 %
LHO, LLO, Virgo	73.4 d	49.9 %
O3: 361.1 d		
LHO	10.1 d	2.8 %
LLO	9.7 d	2.7 %
Virgo	25.0 d	6.9 %
LHO, LLO	48.9 d	13.5 %
LHO, Virgo	31.9 d	8.8 %
LLO, Virgo	39.1 d	10.8 %
LHO, LLO, Virgo	154.3 d	42.7 %
O3GK: 13.7 d		
GEO 600	4.5 d	32.9 %
KAGRA	0.9 d	6.5 %
GEO 600, KAGRA	6.4 d	46.7 %
O4a: 237.0 d		
LHO	33.3 d	14.1 %
LLO	37.0 d	15.6 %
LHO, LLO	126.5 d	53.4 %

an estimate of the distance to which a detector could detect a BNS merger with a signal-to-noise ratio (SNR) of 8 after averaging over sky location and orientation. The variability in the BNS inspiral range over the course of O4a is shown in Figure 1. The plot shows that the observatories frequently operated near their peak sensitivity of around 160 Mpc in O4a. However, there are also times when elevated noise levels cause the sensitivity to drop, as well as times when the detectors are not operating at all or operating for periods too short to make a reliable inspiral range estimate, and in this case the inspiral range is set to zero. This variability in instrument sensitivity is an important feature of the strain data, and needs to be properly accounted for in any analysis. Over the course of O1 through O4, the typical BNS inspiral range of the instruments generally improved for each run due to occasional hardware upgrades and commissioning work at the observatories (Brooks et al. 2021; Driggers et al. 2019; Buikema et al. 2020; Soni et al. 2021; Capote et al. 2025; Jia et al. 2024; Tse et al. 2019; Soni et al. 2024). The evolution of this range is described in Abac et al. (2025a) and Abbott et al. (2020a).

In addition to the strain time series, the observatories also record a large number of auxiliary channels to measure the state of each instrument and the local environment (Nguyen et al. 2021; Huxford et al. 2024). These channels record quantities like laser-power levels, temperatures, seismic motion, angular alignments of mirrors, and many other types of information that can be used to assess instrument performance (Rollins 2016; Soni et al. 2025). A subset of these auxiliary channels is included in the O3 and O4a data releases, and is described in Section 6.

3. CALIBRATION

Ground-based interferometers make use of a feedback control loop in order to hold the differential arm degree of freedom, $\Delta L(t) = \Delta L_x(t) - \Delta L_y(t)$, in resonance. Calibration refers to the process of reconstructing the external differential arm motion $\Delta L(t)$ through a model for the interferometer response function R and the measured error signal from the differential arm feedback loop, d_{err} (Abbott et al. 2017; Viets et al. 2018). In the time domain, the strain can be reconstructed through a convolution of the differential arm error signal and the interferometer response function

$$\Delta L(t) = R(t) \otimes d_{\text{err}}(t), \quad (1)$$

where \otimes represents a convolution, implemented using digital finite impulse response filters for the response function (Viets et al. 2018). The strain $h(t)$ is the ratio of the differential arm motion to the unperturbed interferometer arm length L ,

$$h(t) = \frac{\Delta L(t)}{L}, \quad (2)$$

where L is the length of an interferometer arm and $L \simeq 3995$ m for LIGO.

Imperfect calibration results in small errors in the measured strain values. For LIGO in O4a, the broadband

uncertainty on the calibrated strain data is determined on an hourly cadence using a modified version of the methods described in Sun et al. (2020) that incorporates additional continuous measurements of the calibrated strain systematic error at discrete frequencies (Wade et al. 2025). Calibration uncertainty values for all runs are available in the LIGO Document Control Center (LIGO, Virgo, and KAGRA 2025).

Calibration methods for past observing runs are described in Abbott et al. (2017); Cahillane et al. (2017); Sun et al. (2020, 2021); Chen et al. (2025) and Acernese et al. (2018, 2022). During O4a, the final calibrated-strain data for both LIGO observatories were computed in near-realtime. The photon-calibrator system was used in O4a to inject continuous, sinusoidal excitations at eight frequencies throughout the run (Karki et al. 2016; Bhattacharjee et al. 2024). The systematic error in the calibration at these frequencies was then inferred through the transfer function of the photon-calibrator excitation strain and the reconstructed strain (Wade et al. 2025). The measured systematic error at each of these frequencies was included in the modeled systematic error. The O4a run marked the first time calibration uncertainty estimates were provided for the near-realtime calibrated strain data in LIGO, making this data usable as the final calibrated strain data product. Example uncertainty envelopes for the LHO and LLO calibrated strain data are shown in Figure 2. These envelopes represent the median systematic calibration error as well as the 1σ uncertainty on the systematic error for a one-hour time period during O4a. The black dots overlayed on the envelopes are direct measurements of the calibration systematic error over the one-hour time period using sinusoidal photon-calibrator injections at specific frequencies. The calibrated strain data for LIGO in O4a should be considered valid for analyses within the provided hourly uncertainty envelopes in the range 10–5000 Hz.

4. DATA QUALITY

Noise in the strain data is sometimes approximated as stationary and Gaussian. However, real strain data are also affected by disturbances originating from instrumental and environmental sources (Abbott et al. 2020b; Soni et al. 2025). These artifacts can manifest as broadband, non-Gaussian, short-duration features known as *glitches* (Nuttall 2018; Glanzer et al. 2023), or as narrowband spectral features referred to as *spectral lines* (Covas et al. 2018). In addition, GW observatories can experience periods of degraded performance due to issues in control systems, calibration procedures, or environmental disturbances. These episodes can compromise data quality over extended durations, reducing the sensitivity of the detectors and potentially biasing astrophysical parameter estimation (Pankow et al. 2018; Macas et al. 2022; Kwok et al. 2022; Ghonge et al. 2024). To support robust analyses, LVK employs a suite of data-quality metrics designed to identify and allow mitigation of the impact of instrumental and environmental noise. An overview of LIGO detector characterization efforts

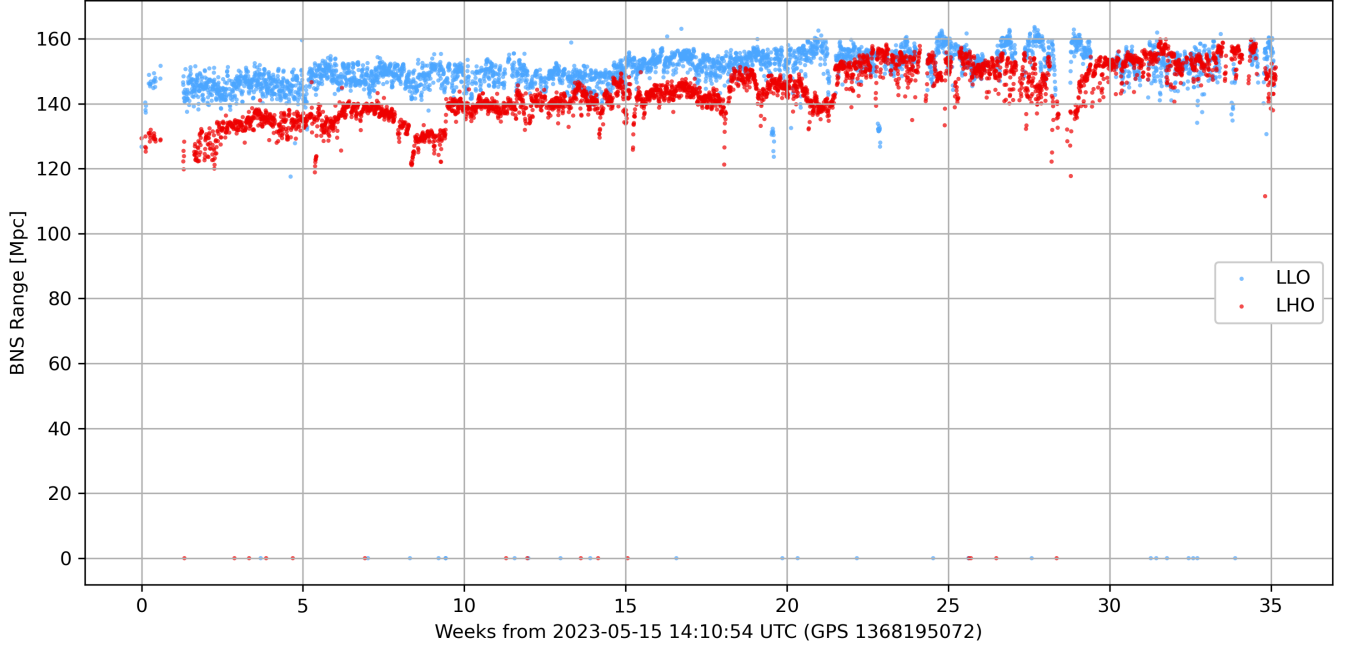


Figure 1. BNS inspiral range over time for O4a. Each point corresponds to a time interval of 4096 seconds, corresponding to the time range of one strain data file. The fast Fourier transform window length used is 8 seconds with a 4 seconds overlap. These inspiral range values are stored as metadata for each file in the GWOSC database and are accessible via the GWOSC website.

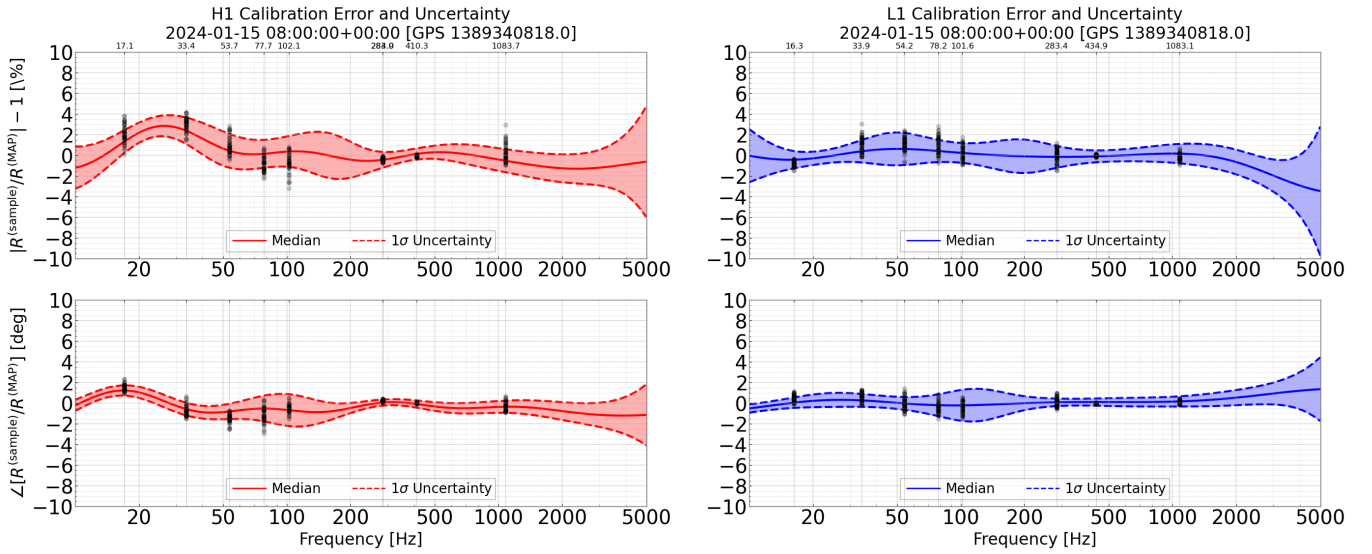


Figure 2. LIGO Hanford (left) and Livingston (right) frequency-dependent calibration error for a one-hour time period in O4a starting at January 15, 2024 08:00:00 UTC. The magnitude of the calibration error is shown in the top plots and the phase of the calibration error (in units of degrees) is shown in the bottom plots. The median systematic error of the calibration is given by the solid line. The 1σ uncertainty on this systematic error is given by the dotted lines. The black dots overlaid on the figure at specific frequencies are direct measurements of the calibration error at a specific frequency during this one-hour time period. These measurements are made using sinusoidal injections with the photon-calibrator system. These uncertainties are representative of typical LIGO calibration uncertainties throughout O4a.

is available in [Soni et al. \(2025\)](#). Detector characterization methods for past observing runs are described in [Davis et al. \(2021\)](#); [Acernese et al. \(2023a\)](#); [Nuttall et al. \(2015\)](#); [Abbott et al. \(2016, 2018\)](#); [Covas et al. \(2018\)](#); [Nguyen et al. \(2021\)](#); [Acernese et al. \(2023b\)](#); and [Akutsu et al. \(2021b\)](#).

Searches for different types of signals exhibit distinct susceptibility to different noise sources, but detector characterization is needed in all cases to remove signals of terrestrial origin and strengthen the confidence of detections. Data-quality products are employed across four broad categories of searches, each with customized detector-characterization methods ([Caudill et al. 2021](#)). Compact binary coalescence (CBC) searches ([Abac et al. 2025c](#)) target GW signals from the coalescence of neutron stars and/or black holes by applying matched-filtering techniques with modeled waveform templates. GW burst (BURST) analyses ([Abac et al. 2025d](#)) aim to identify short-duration transients without strong assumptions on the signal morphology, by detecting excess power in the time–frequency representation of the strain data. Continuous wave (CW) searches ([Abbott et al. 2022a](#)) focus on long-duration, nearly monochromatic signals such as GWs emitted by non-axisymmetric rotating neutron stars. Stochastic (STOCH) searches ([Abbott et al. 2021b](#)) aim to detect a diffuse GW background resulting from the superposition of numerous unresolved sources.

4.1. Hardware Injections

Simulated GW signals, known as *hardware injections* ([Biwer et al. 2017](#)), are introduced by physically displacing the interferometer test masses to mimic true astrophysical events and characterize the performance of the detectors and analyses. Hardware injections with signals that mimic expected astrophysical sources are labeled by the simulation type, corresponding to the different classes of potential sources (CBC, BURST, STOCH, or CW). Detector characterization *safety injections* are labeled as DETCHAR injections. These are used to test couplings between channels used to monitor instrumental and environmental noise sources.

We identify auxiliary channels that can be used to indicate a detector problem, for example, when they display excess noise levels. However, some channels are *unsafe* for identifying noise because they respond to astrophysical signals and therefore a response in the auxiliary channel could indicate a real signal. An auxiliary channel is said to be safe to use for identifying noise transients only if it does not respond to astrophysical signals. Safety injections are used to identify unsafe channels. They are performed by actuating the end test-mass mirror using a photon calibrator, thereby generating a response in the primary strain channel ([Karki et al. 2016](#)). Channels that exhibit a response to these injections are considered unsafe to use for vetoes, and are identified following the method in [Essick et al. \(2021\)](#).

Hardware injection times are available on the GWOSC website as Timelines, with additional notes in the documentation for each data release. In O4a there were no injections labeled CBC, BURST, DETCHAR, or STOCH

during observing mode. The only hardware injections present in the released data are of the CW type and consist of simulations of 18 spinning neutron stars whose parameters are given on the GWOSC website,² with GW frequencies spanning 12–3000 Hz. Injecting simulated CW signals allows, within the uncertainties of the hardware injection system, a direct end-to-end assessment of degradation in CW signal detection due to imperfect calibration or due to noise subtraction. These injections are almost always present (in O4a, only 1.7% of the released LHO data and 2.6% of LLO data do not have CW injections) but because they are faint and nearly monochromatic they have minimal impact on transient-signal searches.

4.2. Data-quality Flags

Data-quality flags are used to identify periods during which the strain data are affected by data-quality issues. These flags are used by analysis pipelines to exclude or down-weight compromised data segments. Flags are classified in order of descending severity, such that the most severe problems are labeled Category 1 (CAT1). These flags mark intervals of time affected by well-understood and severe data-quality issues (hardware faults, control-system failures, or known periods of malfunction) during which the strain data are not considered suitable for astrophysical analyses; these times are systematically excluded from all GW searches and parameter-estimation studies. Some searches also apply the less severe Category 2 (CAT2), which are typically shorter in duration than CAT1 ([Abac et al. 2025c](#)). Category 3 (CAT3) flags are used to identify possible issues of unknown origin which are found through statistical studies.

During O4a, some searches used only the CAT1 flag set. CAT2 flags were applied only to BURST searches. The methodology for identifying and applying these flags during O4a is described in detail in [Soni et al. \(2025\)](#).

For CBC analyses, an additional data quality product used during O4a is the set of statistical flags derived from the `idQ` supervised-learning framework ([Essick et al. 2020](#)). This pipeline evaluates the likelihood that transient noise is present in the strain data based on activity in auxiliary channels that are not expected to be sensitive to astrophysical sources. The `idQ` pipeline produces several statistical outputs sampled at 128 Hz. The low-latency versions of the `idQ` outputs are available in the alternate strain release described in Section 5.5; the corresponding channel names are listed in Table 2. The `OK` flag indicates whether the `idQ` outputs are reliable at a given time, taking the value 1 when valid and 0 otherwise. Other outputs include a normalized RANK score that reflects the raw classifier output, an estimated detection efficiency (EFF), the false alarm probability (FAP) of misclassifying clean times as glitchy, and the log likelihood-ratio (LOGLIKE), where positive values suggest the presence of a glitch and negative values

² O4a Injections, https://gwosc.org/O4/o4_inj

suggest clean data. For CBC searches, the `idQ` flags typically used are derived by thresholding the `LOGLIKE` channel; segments with `LOGLIKE > 5` are flagged as likely to be glitch-contaminated. Unlike `CAT1` and `CAT2` flags, `idQ` flags are not applied universally. Searches algorithms may choose to use them either as vetoes or to re-rank the significance of candidate events.

Table 2. The `idQ` channel names in the alternate strain release described in Section 5.5, sampled at 128 Hz. *Ifo* corresponds to H1 for Hanford or L1 for Livingston and AR stands for Analysis Ready.

	Channel name
OK Flag	<i>Ifo</i> : IDQ-OK_OVL_10_2048_AR
Rank	<i>Ifo</i> : IDQ-RANK_OVL_10_2048_AR
False Alarm Prob.	<i>Ifo</i> : IDQ-FAP_OVL_10_2048_AR
Efficiency	<i>Ifo</i> : IDQ-EFF_OVL_10_2048_AR
Log likelihood-ratio	<i>Ifo</i> : IDQ-LOGLIKE_OVL_10_2048_AR

4.3. Spectral Line Catalog

Spectral lines are narrowband, often persistent features that appear in the amplitude spectral density of GW strain data. These features arise from a variety of instrumental and environmental sources, including mechanical resonances (e.g., violin-mode resonances from the suspension system), injected lines used for calibration, digital dither signals, and harmonics of the electrical mains. Although their impact on CBC and BURST searches is minimal, spectral lines are a significant concern for persistent searches. Spectral artifacts that overlap with the target signal frequency can severely impact CW searches, which rely on coherence over long timescales. Similarly, STOCH searches are sensitive to lines, especially those of common origin or at harmonics of shared noise sources.

To support the identification and mitigation of these features, the LVK maintains a curated catalog of instrumental spectral lines (Covas et al. 2018). The catalog includes both previously known artifacts and newly identified lines, and provides relevant metadata such as frequency, amplitude, detector, and, where possible, a suspected source. This information is used by various search pipelines to identify contaminated frequency bins, apply vetoes, or model noise contamination. Spectral line catalogs are publicly available on the GWOSC website as part of the documentation of each run’s data release.³

4.4. Glitch Subtraction

Glitches represent a significant source of contamination in strain data, particularly affecting transient searches while

having limited impact on persistent searches. In a small number of cases, a glitch occurs in close temporal and spectral proximity to a candidate GW signal, requiring targeted mitigation to reliably recover the astrophysical signal. Subtraction techniques are employed to remove localized excess power in the time–frequency domain (Pankow et al. 2018). One such method is *BayesWave* (Cornish et al. 2021; Hourihane et al. 2022), which models and subtracts transient noise features from the data without requiring a specific model for the astrophysical signal. A complementary method is linear noise subtraction (Davis et al. 2019), which removes known, repeatable noise contributions using information from auxiliary sensors that monitor the detector environment and instrumental systems.

During O4a, 16 candidate events with a false alarm rate (FAR) below 1 per year required such glitch mitigation in at least one interferometer (Abac et al. 2025b). These events are listed in Table 3, along with their GPS time, affected interferometer(s), and the time–frequency region used to constrain the subtraction and assess residuals. All glitch mitigated data listed in Table 3 were produced with the *BayesWave* pipeline.

5. STRAIN DATA

Sections 5.1 to 5.4 describe the *default strain-data release*, which can be downloaded directly from the GWOSC website or accessed via the `fetch_open_data` method of the `gwpy` package (Macleod et al. 2021). Alternatively, especially for downloading large data sets, such as an entire observation run, users can download data from the network data server NDS2 (Zweizig et al. 2021) or the Open Science Data Federation (OSDF) service that acts as a storage resource broker and optimizes data access through a worldwide network of data centers.⁴ While much of the content in this section is similar across observing runs, Section 5.4 describes differences between runs.

Data in the LVK archives are stored as gravitational-wave frame files (gwf; LIGO Scientific Collaboration and Virgo Collaboration 2022), a custom binary format developed within the GW community in which data are uniquely identified by a channel name and a frame type. Files for the default strain-data release are created by repackaging the original LVK data, whose identifiers are listed in Table 4 for all observing runs. The best calibration version available is used in the default strain release. In addition to the default strain-data release, several *alternate strain* channels have also been released starting from O3 (see Section 5.5).

The released calibrated strain data of the observing runs are divided into files containing 4096 seconds of data each. When data are missing or do not meet the necessary quality standards for analysis, strain values are recorded as NaNs. The strain data are available at both the original sampling rate of 16384 Hz and a reduced rate of 4096 Hz, referred as 16 kHz and 4 kHz in the remainder of this paper. The

³ GWOSC data releases, <https://gwosc.org/data>

⁴ Large Scale Data and Computing Resources, <https://gwosc.org/osdf>

Table 3. List of O4a events from [Abac et al. \(2025b\)](#) with FAR < 1 per year, for which glitch subtraction was performed using *BayesWave* ([Cornish et al. 2021](#)). For each event, we provide the GPS time, the interferometer (IFO) where subtraction was applied, and the time and frequency windows used for subtraction. The time window indicates the approximate time of the glitch and is referenced from the indicated GPS time, with negative values before the merger and positive values after the merger.

Event	GPS Time	IFO	Time (s)	Frequency (Hz)
GW230606_004305	1370047403.79	LHO	[1.11, 1.31]	[8.0, 512]
GW230707_124047	1372768865.35	LHO	[−0.15, 0.1]	[15.0, 30.0]
GW230708_053705	1372829843.12	LHO	[−2.02, 0.98]	[10.0, 50.0]
GW230709_122727	1372940865.20	LHO	[−0.9, 0.1]	[15.0, 70.0]
GW230806_204041	1375389659.94	LHO	[1.8, 2.0]	[25.0, 65.0]
GW230819_171910	1376500768.45	LLO	[−3.2, −2.8]	[8.0, 512]
GW230914_111401	1378725259.73	LLO	[1.87, 2.27]	[10.0, 40.0]
GW230914_111401	1378725259.73	LHO	[1.87, 2.27]	[10.0, 40.0]
GW230924_124453	1379594711.84	LHO	[−0.54, −0.34]	[20.0, 40.0]
GW231020_142947	1381860327.78	LLO	[−3.38, −2.73]	[10.0, 30.0]
GW231113_122623	1383913601.88	LLO	[0.01, 0.22]	[70.0, 120.0]
GW231114_043211	1383971549.25	LHO	[−0.95, −0.6]	[10.0, 30.0]
GW231118_090602	1384333580.01	LHO	[−4.81, −4.51]	[15.0, 50.0]
GW231123_135430	1384782888.63	LLO	[−1.7, −1.1]	[15.0, 30.0]
GW231123_135430	1384782888.63	LHO	[−1.7, −1.1]	[15.0, 30.0]
GW231129_081745	1385281083.64	LLO	[1.4, 1.8]	[10.0, 170.0]
GW231221_135041	1387201859.32	LHO	[0.3, 0.4]	[200.0, 450.0]
GW231223_032836	1387337334.05	LHO	[−0.55, −0.25]	[10.0, 25.0]

downsampling process is carried out using the standard decimation method `scipy.signal.decimate`, from the Python library *SciPy* ([Virtanen et al. 2020](#)). Before downsampling, an order 8 Chebyshev type I filter ([Smith 1999](#)) is used as anti-aliasing filter.

The maximum resolvable frequency in a given dataset is constrained by the Nyquist–Shannon sampling theorem ([Nyquist 1924](#)) and corresponds to half of the sampling rate. Due to the roll-off effect of the anti-aliasing filters applied during resampling, the valid frequency range is slightly lower than the Nyquist frequency. Consequently, for data sampled at 4 kHz, frequencies above approximately 1700 Hz are increasingly attenuated by the anti-aliasing filter, which can suppress but not entirely eliminate usable signal content. For data sampled at 16 kHz, however, the limiting factor is given by the calibration which restricts the valid data to 5 kHz, as described in Section 3.

These considerations on the maximum frequency are a crucial factor to consider when selecting a dataset to download. On the other hand, data sampled at higher rates require increased storage space and longer download times. Users should, therefore, select the dataset that best aligns with their specific requirements.

5.1. Structure of the Default Strain-Data Files

The default strain files include not only the strain data but also information on data quality and injections. The main file formats used for the GWOSC open data are the Hierarchical

Data Format (hdf; [Koziol & Robinson 2018](#)), a data format designed for storing and organizing large datasets that is easily readable by many programming languages, and the *gwf* format, which is the file format used in the LVK archives as already mentioned.

For all available file formats, file names in the default strain release contain the following information:

- *Obs*: the observatory, i.e. the site, that is indicated by one letter and can have values L for LIGO Livingston, H for LIGO Hanford, V for Virgo, G for GEO 600 or K for KAGRA.
- *Ifo*: the interferometer label, created by adding a number to the letter that indicates the observatory. This choice allows the identification of multiple detectors installed in the same site, as was the case for Initial LIGO ([Abbott et al. 2009](#)). For the LVK observation runs it can have values H1, L1, V1, G1 or K1.
- *Run*: the observing run name, i.e., O4a.
- *sKHZ* or *s*: the sampling rate in kHz, *s* can have values 4 or 16 (4096 Hz or 16384 Hz).
- *Rn* or *Vn*: release number or version number of the file. The letter V was used only for O1, then it was avoided because it could be confused with the Virgo interferometer name.

Table 4. Channel names and frame types that allow tracing the provenance of strain data released on GWOSC. H1, L1, V1, G1 and K1 are short versions of the interferometer names. The attribute `CLEAN` in H1 and L1 indicates that noise subtraction (Vajente et al. 2020; Davis et al. 2019; Viets & Wade 2021) was used. `AR` stands for Analysis Ready and indicates that these channels contain only data for times ready to be analysed. The other parts of the names refer in general to the calibration version.

Run	IFO	Channel name	Frame type
O1	LHO	H1:DCS-CALIB_STRAIN_C02	H1_HOFT_C02
O1	LLO	L1:DCS-CALIB_STRAIN_C02	L1_HOFT_C02
O2	LHO	H1:DCH-CLEAN_STRAIN_C02	H1_CLEANED_HOFT_C02
O2	LLO	L1:DCH-CLEAN_STRAIN_C02	L1_CLEANED_HOFT_C02
O2	Virgo	V1:Hrec_hoft_V102Repro2A_16384Hz	V102Repro2A
O3a	LHO	H1:DCS-CALIB_STRAIN_CLEAN_SUB60HZ_C01	H1_HOFT_CLEAN_SUB60HZ_C01
O3a	LLO	L1:DCS-CALIB_STRAIN_CLEAN_SUB60HZ_C01	L1_HOFT_CLEAN_SUB60HZ_C01
O3a	Virgo	V1:Hrec_hoft_16384Hz	V1Online
O3a(last two weeks)	Virgo	V1:Hrec_hoft_V103ARepro1A_16384Hz	V103Repro1A
O3b	LHO	H1:DCS-CALIB_STRAIN_CLEAN_SUB60HZ_C01	H1_HOFT_CLEAN_SUB60HZ_C01
O3b	LLO	L1:DCS-CALIB_STRAIN_CLEAN_SUB60HZ_C01	L1_HOFT_CLEAN_SUB60HZ_C01
O3b	Virgo	V1:Hrec_hoft_16384Hz	V1Online
O3GK	GEO 600	G1:DER_DATA_HD_CLEAN	G1_RDS_C02_L3
O3GK	KAGRA	K1:DAC-STRAIN_C20	K1_HOFT_C20
O4a	LHO	H1:GDS-CALIB_STRAIN_CLEAN_AR	H1_HOFT_C00_AR
O4a	LLO	L1:GDS-CALIB_STRAIN_CLEAN_AR	L1_HOFT_C00_AR

- *GPSstart*: the starting time of the data contained in the file, as a 10-digit GPS value (in seconds).
- *Dur*: the duration in seconds of the file, typically 4096 seconds.
- *Ext*: the extension corresponding to the file format (gwf, hdf or txt).

The structure of the file names is:

$$Obs-FrameType-GPSstart-Dur.Ext$$

where the *FrameType* is *Ifo_GWOSC_Run_sKHZ_Rn*.

The `hdf` files contain three folders (or groups): *meta*, *quality* and *strain*.

The folder *meta* hosts the metadata of the file: *Description*, *DescriptionURL*, *Detector* (e.g., L1), *Observatory* (e.g., L), *Duration*, *GPSstart*, *UTCstart* (duration and starting time, using GPS and UTC standards, respectively, of the segment of data contained in a file), *StrainChannel* and *FrameType* used in the LVK archives as listed in Table 4.

The folder *strain* contains the array *Strain* of $h(t)$ values with useful attributes such as *Xstart* and *Xspacing* that define the GPS start time of the data contained in the array and the temporal distance between points in the array.

The folder *quality* contains two subfolders: one for data quality and another for injections. Each subfolder includes a bitmask that indicates, for each second, the status of data quality or injections, along with a description of each bit in the mask (see Section 5.2 for details).

The `gwf` files include three channels: one for strain data, one for data quality, and one for injections. The channel names in the GWOSC `gwf` files are listed in Table 5.

Table 5. Channel names in the GWOSC `gwf` files. The nomenclature is similar to that described for the file name conventions: *Ifo* is the interferometer, *s* is the sampling rate, *n* is the version or release (until now only 1 has been used).

	Channel name
Strain	<i>Ifo</i> :GWOSC- <i>sKHZ_Rn</i> _STRAIN
Data-quality mask	<i>Ifo</i> :GWOSC- <i>sKHZ_Rn</i> _DQMASK
Injections mask	<i>Ifo</i> :GWOSC- <i>sKHZ_Rn</i> _INJMASK

5.2. Data Quality and Injections in GWOSC Files

The data-quality information is encoded in the default strain release as a bitmask following the structure described in Table 6, with a 1 Hz sampling rate.⁵ The meaning of the data-quality flags is explained in Section 4. For template-based binary coalescence searches and minimally modeled searches, labeled respectively as CBC and BURST in Table 6, the bitmask allows 3 categories of data quality (labeled with CAT1, CAT2 and CAT3). We keep this

⁵ See tutorial 3 of https://github.com/gwosc-tutorial/introduction_gwosc_data to learn how to get data-quality information from GWOSC files.

structure even for runs in which not all the categories have been used. This choice avoids confusion that could arise if the same bit would have different meaning in different runs. A bit value of 1 indicates the data has passed both the indicated level and lower-level checks; for example, a 1 in the CBC_CAT2 bit indicates the data pass both CBC_CAT1 and CBC_CAT2.

The data-quality bit labeled as DATA is obtained requiring that both CBC_CAT1 and BURST_CAT1 are satisfied. This is the criterion that defines what data are released in the *default strain-data release*.

In O4a, two additional bits have been added to accommodate Category 1 data quality for STOCH searches (STOCH_CAT1) and for CW searches (CW_CAT1). Moreover, the Categories 2 and 3 have not been used for the CBC data-quality flag so the corresponding segments coincide with those marked as CBC_CAT1 (and also DATA in this case). BURST searches in O4a did not apply any Category 3 flags. The CW data-quality flag CW_CAT1 is identical to CBC_CAT1.

Table 6. Meaning of the bits in the data-quality bitmask of the GWOSC files. Each bit has value 1 if the data quality passes the corresponding data quality requirement, otherwise the value is zero. Bits 7 and 8 were introduced in O4 and are not present in previous runs (Abbott et al. 2021a, 2023a).

Bit	Short name	Description
0	DATA	Data present
1	CBC_CAT1	Pass CAT1 test for CBC search
2	CBC_CAT2	Pass CAT1 and CAT2 test for CBC search
3	CBC_CAT3	Pass CAT1 and CAT2 and CAT3 test for CBC search
4	BURST_CAT1	Pass CAT1 test for BURST search
5	BURST_CAT2	Pass CAT1 and CAT2 test for BURST search
6	BURST_CAT3	Pass CAT1 and CAT2 and CAT3 test for BURST search
7	STOCH_CAT1	Pass CAT1 test for STOCH search
8	CW_CAT1	Pass CAT1 test for CW search

As discussed in Section 4, a crucial way to test the response of the detector is the use of *hardware injections*. In GWOSC files the information about injections is provided as 1 Hz time series containing a bitmask detailed in Table 7.⁶ Five bits are used to distinguish injections relevant for astrophysical searches or detector-characterization studies.

Table 7. Meaning of the bits in the injections bitmask of the GWOSC files. The mask indicates when injections are not present, so the bit value is set to 1 to indicate no injection and 0 when there is an injection. HW_INJ stands for hardware injection.

Bit	Short name	Description
0	NO_CBC_HW_INJ	No CBC injections
1	NO_BURST_HW_INJ	No BURST injections
2	NO_DETCHAR_HW_INJ	No DETCHAR injections
3	NO_CW_HW_INJ	No CW injections
4	NO_STOCH_HW_INJ	No STOCH injections

5.3. Additional Segments in the O4a Strain-Data Release

The O4a run started on 24 May 2023 at 15:00 UTC. However, a few segments of data from the engineering run just prior to the start of the run were used in the search for GW emitted from SN 2023ixf (Abac et al. 2025e) and for the neutron star–black hole binary candidate GW230518_125908 (Abac et al. 2025b), and they have been added to this release. These additional data segments span between times 15 May 2023 14:13:22 UTC (GPS 1368195220) and 19 May 2023 17:31:33 UTC (GPS 1368552711) when both LHO and LLO were in observing mode. These segments have a total duration of 0.8 days. Including this addition, the total amount of observing time in O4a is 160.8 days for LHO and 164.3 days for LLO (to compare with Table 1, 0.8 days have to be added to the coincident times). Using this total amount of time as reference, the percentage of the observing time for which the data quality pass each category described in Table 6 in O4a can be calculated. Since these percentages are close to 100%, Table 8 summarizes the percentages of failing times.

Table 8. Percentage of the observing time in O4a, including the extra 0.8 days of engineering run data, for which data quality fail the categories described in Table 6.

Short name	Percentage in LHO	Percentage in LLO
DATA	0.0971%	0.0059%
CBC_CAT1	0.0971%	0.0059%
CBC_CAT2	0.0971%	0.0059%
CBC_CAT3	0.0971%	0.0059%
BURST_CAT1	0.0971%	0.0059%
BURST_CAT2	0.2242%	0.1188%
BURST_CAT3	0.2242%	0.1188%
STOCH_CAT1	0.0979%	0.0065%
CW_CAT1	0.0971%	0.0059%

⁶ See tutorials in <https://gwosc.org/tutorials/> to learn how to get hardware injections information from GWOSC files.

5.4. Previous Runs Data Releases

The structure described here for the default strain data is largely valid for all data released to date (Abbott et al. 2021a, 2023a), with few differences. These concern details in the naming conventions of the files and the channels within them. For example, the *FrameType* mentioned in Section 5.1 is *Ifo_LOSC_s_Vn* in O1, the *StrainChannel* and *FrameType* have been present in files since O2, while the channel names in the *gwf* files used only in O1 are shown in Table 9.

The main difference that the user will notice is that up to O3, for each published GW detection, data snippets centered on the event detection time are also released via the GWOSC Event Portal, described in Section 7. These data snippets are provided as plain-text files in addition to the *hdf* and *gwf* files described above. The text files contain strain values in a single column. As of O4, data snippets for most events are no longer published, but instead the associated files from the default strain-data release are linked for each event in the Event Portal, if available at the time of posting the event.

Table 9. Channel names in the GWOSC *gwf* files, used only in O1 for the 4 kHz release (*Ifo* is the interferometer name).

	Channel name
Strain	<i>Ifo</i> :LOSC-STRAIN
Data-quality mask	<i>Ifo</i> :LOSC-DQMASK
Injections mask	<i>Ifo</i> :LOSC-INJMASK

5.5. Alternate Strain Release

The default strain files described in Sections 5.1–5.4 are prepared after each observing run in order to provide a user-friendly file format that includes the preferred strain channel and the final data quality and injection segments. For O3 and O4a, in addition to these user-friendly files, each data release also includes an alternate strain release, which includes several versions of the strain channel and more closely matches the data available to LVK members before the data release. Detailed documentation is available on the GWOSC website (LIGO Scientific Collaboration, Virgo Collaboration and KAGRA Collaboration 2021a,b, 2025).

Alternate strain releases from O3 and O4a are available for all times the detectors passed the conditions for ANALYSIS_READY, meaning that the detectors were nominally in a good working state. This set of times includes a small amount of time that fails CAT1 data quality, and so there are some times in the alternate strain releases that are not available in the default strain files. Files and strain channels are marked with the tag AR, to indicate that only ANALYSIS_READY times are included. For O3, this release was prepared after the run had ended, with three channels of varying noise subtraction levels for LIGO, and two channels for Virgo: a main and a short-duration one covering a period when additional noise subtraction was needed (Abbott et al. 2023a).

Starting in O4a, the AR frames are produced during the run. A calibration pipeline runs at all times and writes out strain data in one second long frame files in order to produce low-latency strain data, including the preferred channel GDS-CALIB_STRAIN_CLEAN. Low-latency analyses, include pipelines that produce public transient alerts, use these low-latency frame files. To produce the AR frames, a frame aggregator collects the one second files into ANALYSIS_READY frame files of up to 4096 seconds long, excludes any times that are not marked as ready for analysis, and adds the tag AR to the channel names. The AR frame files are then used for most offline LVK analyses, so that the released product exactly matches data used inside the collaboration.

The alternate strain releases are not currently available for direct download from the GWOSC website; instead, they are available via OSDF and NDS2, as discussed earlier in Section 5.

The O4a alternate strain release includes four versions of the strain channel for each LIGO instrument, which are summarized in Table 10 and described below. In addition to the strain channels, the O4a ANALYSIS_READY frames also include a number of auxiliary channels that record data-quality information and calibration parameters. The O4a strain channels are (*Ifo* corresponds to H1 for Hanford or L1 for Livingston):

- *Ifo*:GDS-CALIB_STRAIN_AR This is the calibrated strain data with no noise subtraction applied and corresponds to the channel name DCS-CALIB_STRAIN_C01_AR in O3 (Abbott et al. 2023a).
- *Ifo*:GDS-CALIB_STRAIN_NOLINES_AR This is the calibrated strain data after removing narrowband noise. This channel removes the calibration lines, 60 Hz power-mains line, and harmonics of the power-mains line as described in Viets & Wade (2021). It corresponds to the channel name DCS-CALIB_STRAIN_CLEAN_C01_AR in O3 (Abbott et al. 2023a).
- *Ifo*:GDS-CALIB_STRAIN_CLEAN_AR This is the calibrated strain data, after subtracting both narrowband and broadband noise. This applies additional broadband noise subtraction on to the *Ifo*:GDS-CALIB_STRAIN_NOLINES_AR channel, using the method described in Vajente et al. (2020). This is the recommended channel for transient searches, and it corresponds to the channel name DCS-CALIB_STRAIN_CLEAN_SUB60HZ_C01_AR in O3 (Abbott et al. 2023a).
- *Ifo*:GDS-GATED_STRAIN_AR This is the *Ifo*:GDS-CALIB_STRAIN_NOLINES_AR channel where times with loud glitches are replaced with zeros by applying a window function around short segments of elevated noise (Zweizig & Riles 2020; Usman et al.

Table 10. Alternate strain channels in the O4a release and the layers of noise subtraction applied to them. `NOLINES` means that narrowband noise features have been subtracted, while `CLEAN` means that broadband noise features have also been subtracted and `GATED` means the removal of loud glitches.

Channel name	Narrowband noise subtraction	Broadband noise subtraction	Glitch removal
<i>Ifo</i> :GDS-CALIB_STRAIN_AR			
<i>Ifo</i> :GDS-CALIB_STRAIN_NOLINES_AR	✓		
<i>Ifo</i> :GDS-CALIB_STRAIN_CLEAN_AR	✓	✓	
<i>Ifo</i> :GDS-GATED_STRAIN_AR	✓		✓

2016). This channel was not used for analyses by the LVK.

During some intervals of O4a, the broadband-noise subtraction was turned off, so that the channels *Ifo*:GDS-CALIB_STRAIN_NOLINES_AR and *Ifo*:GDS-CALIB_STRAIN_CLEAN_AR contained identical data. At LHO, broadband noise subtraction was turned off from 21 June 2023 16:00 UTC until 11 November 2023 01:00:00 UTC. At LLO, this period was from 24 May 2023 15:00:00 UTC until 10 November 2023 23:00:00 UTC.

6. AUXILIARY CHANNELS

In addition to the strain time series, LIGO records around 200,000 *auxiliary channels* for each instrument. Auxiliary channels are stored as time series data and record the state of the instrument, the local environment, and a number of digital-filter settings. Auxiliary channels include readings from seismometers, accelerometers, photodiodes, magnetometers, wind monitors, and microphones (Nguyen et al. 2021; Huxford et al. 2024).

The O3 and O4a data releases include the set of LIGO auxiliary channels used for noise subtraction and to produce data-quality flags. The auxiliary data release consists of about 40 channels for each LIGO detector for each run. The online documentation includes the name of each available channel along with the associated sampling rate and a short description of the channel content.⁷

Auxiliary channels should be used with caution, as the data are not necessarily calibrated and may include times when the data values are missing or corrupt. For example, sensors sometimes break or become disconnected leading to periods of corrupted data. Auxiliary data are available at all times when the detector is in `ANALYSIS_READY` with the exact times marked in segment lists that are available with the data release documentation.

In addition to channels used for noise subtraction and data-quality flags, some auxiliary data has been released on request and are now available on the GWOSC website. For O3, these releases include a data set to support a study of machine learning applied to detector characterization

(Gurav et al. 2024), and a study of noise-subtraction methods (Zackay et al. 2023).

Auxiliary-channel data cannot currently be downloaded directly through the GWOSC website or the API. Instead, auxiliary-channel data are available through the NDS2 and OSDF interfaces described in Section 5.

7. EVENT PORTAL

The GWOSC Event Portal provides an online interface to a database of published GW transient events.⁸ These events are short-duration GW signals identified in the strain data by search analyses. They are typically attributed to a signal consistent with a CBC source. Not all events in the Event Portal will be from CBCs, some may be noise with an instrumental origin.

Users of the Event Portal can discover an array of data products associated with each event, including strain data, segment lists, detection confidence, astrophysical source parameters, and documentation. In most cases, the database also includes links to additional analysis products, such as posterior samples describing source properties and source localizations.

The Event Portal may be accessed as browsable HTML webpages or via a REST API. A Python client, named `gwosc`, can be used to query the API and download content.⁹ Documentation of the Event Portal and REST API are available on the GWOSC website.

7.1. User Interfaces to the Data

A collection of GW transients in the Event Portal is labeled a *release*. A release might be a set of events published in a single paper, such as the new CBC candidates added for GWTC-4.0 (Abac et al. 2025a), or a collection of events that are related in some other way, such as all the GW transients published in stand-alone discovery papers such as the O3 observing run. As a result there are a number of ways to interact with the data through the Event Portal.

The *Release List View* in the Event Portal displays a list of all available releases, summarized in Table 11. Several releases are labeled marginal, i.e., GWTC-1-marginal, GWTC-2.1-marginal,

⁷ See <https://gwosc.org/O3/auxiliary/> for O3 and https://gwosc.org/O4/o4a_auxiliary/ for O4a.

⁸ GWOSC Event Portal, <https://gwosc.org/eventapi>

⁹ GWOSC Client API, <https://pypi.org/project/gwosc/>

GWTC-3-marginal, O3_IMBH_marginal, which include candidate triggers that have a plausible instrumental origin, falling short of the criteria required for the event to be labeled as confident.

In addition, there is one release, GWTC-2.1-auxiliary, in which revised analyses in GWTC-2.1 (Abbott et al. 2024) resulted in the demotion of events that were previously identified in GWTC-2 (Abbott et al. 2021c) as statistically significant. They are included separately for completeness.

With the exception of GWTC-4.0, events available in the individual releases are documented in the tables found in the publications that first reported the events. In the case of GWTC-4.0 the events found in the Event Portal satisfy

$$p_{\text{astro}} > 0.5 \text{ or } \text{FAR} < 1 \text{ yr}^{-1} \quad (3)$$

where p_{astro} is the probability that a GW candidate is of astrophysical origin and FAR is the false alarm rate (the rate of noise triggers with a detection statistic at least as high as the candidate).

Detailed documentation and references to publications are available for each release on the GWOSC website.

By selecting one of the releases, an *Event List* table is generated showing all events in the release, along with source parameters and credible intervals where available. The Event List view includes estimates of a number of physical parameters, such as mass, distance, and spin, as well as search-pipeline outputs such as SNR and FAR. If more than one parameter-estimation analysis is available for any event, then values from the analysis marked as Default PE for the specific event are displayed in the Event List to indicate which of the multiple results are captured in the table. Additionally, the lowest FAR and highest probability of astrophysical origin p_{astro} from all available search-analysis results are included in the Event List table.

A special case of the Event List view is the electronic version of the GWTC, a collection of GW candidates identified by the LVK (Abac et al. 2025a). Selecting the GWTC option returns this set of events as an Event List. It includes confidently detected events from multiple data releases.

Event Lists are also available to browse specific events using customized queries. Event Lists may include more than one version of an event, as some events have appeared in multiple publications, or have been re-analysed with newer code or models. The *Query Page* presents the user with a form that allows selection of events based on name, membership in particular releases, various ranges of masses, distance, redshift, effective inspiral spin (χ_{eff}), p_{astro} , SNR, FAR, UTC and GPS times. The query also allows specification of the output format to return, with support for HTML, JSON, CSV and ASCII (see Figure 3).

The *Single Event View* shows key parameters for an individual event in the Event Portal. The view can include sets of parameters from different pipelines, including search-pipeline outputs such as SNR and FAR, and inferred source properties such as masses and spins. The Single Event View also includes images showing a spectrogram (Chatterji

2005) of the strain data for each detector at the time of the event, and links to download the associated strain time series in multiple file formats, as described in Section 5. The Single Event View also provides links to documentation, low-latency information in Gravitational-Wave Candidate Event Database (GraceDB),¹⁰ General Coordinates Network (GCN) Circulars and Notices, and links to segment lists for times around the event (see Section 5.2 for details). A new feature found on these pages is the Event Viewer which leads to a web app that generates plots of waveforms, source parameters and sky localization for each GW event.¹¹

7.2. Parameter-Estimation Results

Most events in the Event Portal include one or more sets of credible intervals drawn from the publication associated with the event. The naming of parameters is based on the LVK standard names convention.¹² Many entries include multiple sets of values attributed to different priors, waveforms, or analysis changes (Abac et al. 2025c). In some cases, a publication will present credible intervals describing samples combined from several analyses using different waveform models. The results for any individual parameter are expressed as the median value with its 90% symmetric credible interval. Details regarding how the posterior samples were constructed can be found in the publication from which the event is released or in the supplemental releases linked from the Single Event View.

7.3. Supplemental Data Releases

For most events, the Single Event View includes links to supplemental data. These data vary between releases, but in general will include links to the parameter-estimation posterior samples, source localization, and additional resources. Supplemental data releases are published either in the LIGO Document Control Center¹³ or under the LVK Zenodo Community.¹⁴ In addition, GWOSC maintains a snapshot of the Event Portal’s version history as a dataset available on Zenodo.¹⁵ Each snapshot consists of JSON files downloaded from the Event Portal with data for each event.

7.4. Community Catalogs

The Event Portal has recently been extended to provide GW events from catalog authors outside of the LVK, which are collectively organized as *Community Catalogs*. The presentation of results for Community Catalogs is identical to that available with any LVK release of events, adhering to the

¹⁰ GraceDB website, <https://gracedb.ligo.org/>

¹¹ GW Event Viewer, <https://peviewer.lgw.org>

¹² Parameter Estimation Name Standard, <https://lscsoft.docs.ligo.org/pesummary/stable/gw/parameters.html>

¹³ Public LIGO Document Control Center, <https://dcc.ligo.org/cgi-bin/DocDB/DocumentDatabase>

¹⁴ LVK Zenodo Data Releases, <https://zenodo.org/communities/ligo-virgo-kagra/>

¹⁵ GWOSC Zenodo Event Portal Snapshots, <https://zenodo.org/records/10071492>

Table 11. List of releases currently available under the GWOSC Event Portal.^a

Release Name	Notes
GWTC	Cumulative set of GW transients maintained by the LVK (Abac et al. 2025a)
Initial_LIGO_Virgo	Event release from initial LIGO and Virgo, 2005–2010 (Abadie et al. 2012)
O1_O2-Preliminary	Notable events in O1 and O2 published prior to GWTC-1 release (Abbott et al. 2019)
GWTC-1-confident	Confident detections from the O1 and O2 runs (Abbott et al. 2019)
GWTC-1-marginal	Marginal candidates from O1 and O2 runs (Abbott et al. 2019)
GWTC-2	Confident detections from the O3a run (Abbott et al. 2021c)
GWTC-2.1-confident	Confident detections from O3a run based on a revised analysis (Abbott et al. 2024)
GWTC-2.1-marginal	Marginal candidates from O3a run based on a revised analysis (Abbott et al. 2024)
GWTC-2.1-auxiliary	Candidates from GWTC-2 that were demoted in GWTC-2.1 (Abbott et al. 2021c)
GWTC-3-confident	Confident detection from O3b run (Abbott et al. 2023b)
GWTC-3-marginal	Marginal candidates from O3b run (Abbott et al. 2023b)
IAS-O3a	Events from O3a as described in a community catalog (Olsen et al. 2022)
O3_Discovery_Papers	Notable events in O3 run published independently (Abbott et al. 2020c,d,e,f, 2021d)
O3_IMBH_marginal	Marginal intermediate-mass black hole candidates from O3 run (Abbott et al. 2022b)
O4_Discovery_Papers	Notable events in O4 run published independently (Abac et al. 2024; Collaboration et al. 2025)
GWTC-4.0	All events from O4a data product release (Abac et al. 2025b)

^a GWOSC Event Portal, <https://gwosc.org/eventapi/html>

website layout and search capabilities discussed previously. This is achieved by standardizing on a JSON schema file format for GWOSC staff to use to ingest search and parameter-estimation values. The details for this standard JSON are publicly available in GitHub,¹⁶ along with useful test scripts, notebooks, and documentation. The criteria for authors outside the LVK to have their catalogs included in GWOSC is documented in the *GWOSC Community Catalogs Guidelines*.¹⁷

8. SUMMARY

Data from LIGO recorded during O4a are now publicly available through the GWOSC website at gwosc.org. This paper can serve as a practical guide for users interested in analyzing this set of open data. It provides important details about calibration and data quality, explains the structure of the datasets available online, and offers instructions for using the Event Portal, which gives access to the list of astrophysical sources identified by the LVK.

Making these resources available maximizes the scientific potential of the dataset. The O4a data contain a wealth of compact object mergers, many of which are listed in version 4.0 of the Gravitational-Wave Transient Catalog (Abac et al. 2025b). By releasing the data publicly, the community is empowered to further explore and discover new insights.

The present release covers only the first part of the O4 observing run. The second and third parts are planned for

release in May and December of 2026, respectively (LIGO Laboratory 2025). With these forthcoming datasets, we anticipate even more opportunities for discovery.

ACKNOWLEDGEMENTS

This material is based upon work supported by NSF’s LIGO Laboratory, which is a major facility fully funded by the National Science Foundation. The authors also gratefully acknowledge the support of the Science and Technology Facilities Council (STFC) of the United Kingdom, the Max-Planck-Society (MPS), and the State of Niedersachsen/Germany for support of the construction of Advanced LIGO and construction and operation of the GEO 600 detector. Additional support for Advanced LIGO was provided by the Australian Research Council. The authors gratefully acknowledge the Italian Istituto Nazionale di Fisica Nucleare (INFN), the French Centre National de la Recherche Scientifique (CNRS) and the Netherlands Organization for Scientific Research (NWO) for the construction and operation of the Virgo detector and the creation and support of the EGO consortium. The authors also gratefully acknowledge research support from these agencies as well as by the Council of Scientific and Industrial Research of India, the Department of Science and Technology, India, the Science & Engineering Research Board (SERB), India, the Ministry of Human Resource Development, India, the Spanish Agencia Estatal de Investigación (AEI), the Spanish Ministerio de Ciencia, Innovación y Universidades, the European Union NextGenerationEU/PRTR (PRTR-C17.I1), the ICSC - Centro Nazionale di Ricerca in High Performance Computing, Big Data and Quantum Computing, funded

¹⁶ GWOSC Github Community Catalog Schema, <https://github.com/gwosc-tutorial/gwosc-catalog>

¹⁷ GWOSC Community Catalogs Guidelines, <https://dcc.ligo.org/LIGO-M2500012/public>

Query Events

Event Name:

The (partial) name of the event, e.g. GW150914

Release:

Initial_LIGO_Virgo

GWTC-1-confident

GWTC-1-marginal

O1_O2-Preliminary

Restrict search to a Catalog Release

i

Mass 1 Range:

0

∞

i

Mass 2 Range:

0

∞

i

Total Mass Range:

0

∞

i

Final Mass Range:

0

∞

i

Chirp Mass Range:

0

∞

i

Detector Frame Chirp Mass Range:

0

∞

i

Distance (Mpc) Range:

0

∞

i

Redshift Range:

0

∞

i

Network SNR Range:

0

∞

i

χ_{eff} Range:

-1

1

i

False Alarm Rate Range:

0

∞

i

P_{astro} Range:

0

1

UTC Time Range:

GPS Time Range:

Show only last version

Output Format:

HTML

JSON

CSV

ASCII

Submit Query

Figure 3. Event Query Form—A user interface allowing custom selection of events based an selectable attributes.

by the European Union NextGenerationEU, the Comunitat Autònoma de les Illes Balears through the Conselleria d'Educació i Universitats, the Conselleria d'Innovació, Universitats, Ciència i Societat Digital de la Generalitat Valenciana and the CERCA Programme Generalitat de Catalunya, Spain, the Polish National Agency for Academic Exchange, the National Science Centre of Poland and the European Union - European Regional Development Fund; the Foundation for Polish Science (FNP), the Polish Ministry of Science and Higher Education, the Swiss National Science Foundation (SNSF), the Russian Science Foundation, the European Commission, the European Social Funds (ESF), the European Regional Development Funds (ERDF), the

Royal Society, the Scottish Funding Council, the Scottish Universities Physics Alliance, the Hungarian Scientific Research Fund (OTKA), the French Lyon Institute of Origins (LIO), the Belgian Fonds de la Recherche Scientifique (FRS-FNRS), Actions de Recherche Concertées (ARC) and Fonds Wetenschappelijk Onderzoek - Vlaanderen (FWO), Belgium, the Paris Île-de-France Region, the National Research, Development and Innovation Office of Hungary (NKFIH), the National Research Foundation of Korea, the Natural Sciences and Engineering Research Council of Canada (NSERC), the Canadian Foundation for Innovation (CFI), the Brazilian Ministry of Science, Technology, and Innovations, the International Center for Theoretical

Physics South American Institute for Fundamental Research (ICTP-SAIFR), the Research Grants Council of Hong Kong, the National Natural Science Foundation of China (NSFC), the Israel Science Foundation (ISF), the US-Israel Binational Science Fund (BSF), the Leverhulme Trust, the Research Corporation, the National Science and Technology Council (NSTC), Taiwan, the United States Department of Energy, and the Kavli Foundation. The authors gratefully acknowledge the support of the NSF, STFC, INFN and CNRS for provision of computational resources.

This work was supported by MEXT, the JSPS Leading-edge Research Infrastructure Program, JSPS Grant-in-Aid for Specially Promoted Research 26000005, JSPS Grant-in-Aid for Scientific Research on Innovative Areas 2402: 24103006, 24103005, and 2905: JP17H06358, JP17H06361 and JP17H06364, JSPS Core-to-Core Program A. Advanced Research Networks, JSPS Grants-in-Aid for Scientific Research (S) 17H06133 and 20H05639, JSPS Grant-in-Aid for Transformative Research Areas (A) 20A203: JP20H05854, the joint research program of the Institute for Cosmic Ray Research, University of Tokyo, the National Research Foundation (NRF), the Computing Infrastructure Project of the Global Science experimental Data hub Center (GSDC) at KISTI, the Korea Astronomy and Space Science Institute (KASI), the Ministry of Science and ICT (MSIT) in Korea, Academia Sinica (AS), the AS Grid Center (ASGC) and the National Science and Technology Council (NSTC) in Taiwan under grants including the Science Vanguard

Research Program, the Advanced Technology Center (ATC) of NAOJ, and the Mechanical Engineering Center of KEK.

Additional acknowledgements for support of individual authors may be found in the following document:

<https://dcc.ligo.org/LIGO-M2300033/public>.

For the purpose of open access, the authors have applied a Creative Commons Attribution (CC BY) license to any Author Accepted Manuscript version arising. We request that citations to this article use 'A. G. Abac *et al.* (LIGO-Virgo-KAGRA Collaboration), ...' or similar phrasing, depending on journal convention.

Software: This software infrastructure used to publish data products onto the GWOSC website made significant use of the IGWN Software Environment ([IGWN Computing and Software Working Group 2025](#)) curated by the LVK to provide a reproducible computing environment built around tools needed for GW data analysis. Plots were prepared with `Matplotlib` ([Hunter 2007](#)).

DATA AVAILABILITY

All data products described in this work are publicly available on the Gravitational Wave Open Science Center,¹⁸ the Zenodo LVK community page,¹⁹ and through the OSDF and NDS2 data repositories, as described in the previous sections of this paper. Data products are provided under a Creative Commons Attribution 4.0 International license.²⁰

REFERENCES

- Aasi, J., et al. 2015, *Class. Quant. Grav.*, 32, 074001, doi: [10.1088/0264-9381/32/7/074001](https://doi.org/10.1088/0264-9381/32/7/074001)
- Abac, A. G., et al. 2024, *Astrophys. J. Lett.*, 970, L34, doi: [10.3847/2041-8213/ad5beb](https://doi.org/10.3847/2041-8213/ad5beb)
- . 2025a, To be published in this issue. <https://dcc.ligo.org/LIGO-P2400293/public>
- . 2025b, To be published in this issue. <https://dcc.ligo.org/LIGO-P2400386/public>
- . 2025c, To be published in this issue. <https://dcc.ligo.org/LIGO-P2400300/public>
- . 2025d. <https://arxiv.org/abs/2507.12374>
- . 2025e, *Astrophys. J.*, 985, 183, doi: [10.3847/1538-4357/adc681](https://doi.org/10.3847/1538-4357/adc681)
- Abadie, J., et al. 2012, *Phys. Rev. D*, 85, 082002, doi: [10.1103/PhysRevD.85.082002](https://doi.org/10.1103/PhysRevD.85.082002)
- Abbott, B. P., et al. 2009, *Rept. Prog. Phys.*, 72, 076901, doi: [10.1088/0034-4885/72/7/076901](https://doi.org/10.1088/0034-4885/72/7/076901)
- . 2016, *Class. Quant. Grav.*, 33, 134001, doi: [10.1088/0264-9381/33/13/134001](https://doi.org/10.1088/0264-9381/33/13/134001)
- . 2017, *Phys. Rev. D*, 95, 062003, doi: [10.1103/PhysRevD.95.062003](https://doi.org/10.1103/PhysRevD.95.062003)
- . 2018, *Class. Quant. Grav.*, 35, 065010, doi: [10.1088/1361-6382/aaaafa](https://doi.org/10.1088/1361-6382/aaaafa)
- . 2019, *Phys. Rev. X*, 9, 031040, doi: [10.1103/PhysRevX.9.031040](https://doi.org/10.1103/PhysRevX.9.031040)
- . 2020a, *Living Rev. Rel.*, 23, 3, doi: [10.1007/s41114-020-00026-9](https://doi.org/10.1007/s41114-020-00026-9)
- . 2020b, *Class. Quant. Grav.*, 37, 055002, doi: [10.1088/1361-6382/ab685e](https://doi.org/10.1088/1361-6382/ab685e)
- . 2020c, *Astrophys. J. Lett.*, 892, L3, doi: [10.3847/2041-8213/ab75f5](https://doi.org/10.3847/2041-8213/ab75f5)
- Abbott, R., et al. 2020d, *Phys. Rev. D*, 102, 043015, doi: [10.1103/PhysRevD.102.043015](https://doi.org/10.1103/PhysRevD.102.043015)
- . 2020e, *Astrophys. J. Lett.*, 900, L13, doi: [10.3847/2041-8213/aba493](https://doi.org/10.3847/2041-8213/aba493)
- . 2020f, *Astrophys. J. Lett.*, 896, L44, doi: [10.3847/2041-8213/ab960f](https://doi.org/10.3847/2041-8213/ab960f)
- . 2021a, *SoftwareX*, 13, 100658, doi: [10.1016/j.softx.2021.100658](https://doi.org/10.1016/j.softx.2021.100658)
- ¹⁸ GWOSC Home Page: <https://gwosc.org>
- ¹⁹ Zenodo LVK Community Page: <https://zenodo.org/communities/ligo-virgo-kagra/>
- ²⁰ CC BY 4.0 license: <https://creativecommons.org/licenses/by/4.0/>

- . 2021b, Phys. Rev. D, 104, 022004, doi: [10.1103/PhysRevD.104.022004](https://doi.org/10.1103/PhysRevD.104.022004)
- . 2021c, Phys. Rev. X, 11, 021053, doi: [10.1103/PhysRevX.11.021053](https://doi.org/10.1103/PhysRevX.11.021053)
- . 2021d, Astrophys. J. Lett., 915, L5, doi: [10.3847/2041-8213/ac082e](https://doi.org/10.3847/2041-8213/ac082e)
- . 2022a, Phys. Rev. D, 106, 102008, doi: [10.1103/PhysRevD.106.102008](https://doi.org/10.1103/PhysRevD.106.102008)
- . 2022b, Astron. Astrophys., 659, A84, doi: [10.1051/0004-6361/202141452](https://doi.org/10.1051/0004-6361/202141452)
- . 2023a, Astrophys. J. Suppl., 267, 29, doi: [10.3847/1538-4365/acdc9f](https://doi.org/10.3847/1538-4365/acdc9f)
- . 2023b, Phys. Rev. X, 13, 041039, doi: [10.1103/PhysRevX.13.041039](https://doi.org/10.1103/PhysRevX.13.041039)
- . 2024, Phys. Rev. D, 109, 022001, doi: [10.1103/PhysRevD.109.022001](https://doi.org/10.1103/PhysRevD.109.022001)
- Acernese, F., et al. 2015, Class. Quant. Grav., 32, 024001, doi: [10.1088/0264-9381/32/2/024001](https://doi.org/10.1088/0264-9381/32/2/024001)
- . 2018, Class. Quant. Grav., 35, 205004, doi: [10.1088/1361-6382/aadf1a](https://doi.org/10.1088/1361-6382/aadf1a)
- . 2022, Class. Quant. Grav., 39, 045006, doi: [10.1088/1361-6382/ac3c8e](https://doi.org/10.1088/1361-6382/ac3c8e)
- . 2023a, Class. Quant. Grav., 40, 185006, doi: [10.1088/1361-6382/acd92d](https://doi.org/10.1088/1361-6382/acd92d)
- . 2023b, Class. Quant. Grav., 40, 185005, doi: [10.1088/1361-6382/acdf36](https://doi.org/10.1088/1361-6382/acdf36)
- Affeldt, C., et al. 2014, Class. Quant. Grav., 31, 224002, doi: [10.1088/0264-9381/31/22/224002](https://doi.org/10.1088/0264-9381/31/22/224002)
- Akutsu, T., et al. 2021a, PTEP, 2021, 05A101, doi: [10.1093/ptep/ptaa125](https://doi.org/10.1093/ptep/ptaa125)
- Akutsu, T., Ando, M., Arai, K., et al. 2021b, Progress of Theoretical and Experimental Physics, 2021, 05A102, doi: [10.1093/ptep/ptab018](https://doi.org/10.1093/ptep/ptab018)
- Bhattacharjee, D., Savage, R. L., Bajpai, R., et al. 2024, Metrologia, 61, 054002, doi: [10.1088/1681-7575/ad615f](https://doi.org/10.1088/1681-7575/ad615f)
- Biwer, C., et al. 2017, Phys. Rev. D, 95, 062002, doi: [10.1103/PhysRevD.95.062002](https://doi.org/10.1103/PhysRevD.95.062002)
- Brooks, A. F., et al. 2021, Appl. Opt., 60, 4047, doi: [10.1364/AO.419689](https://doi.org/10.1364/AO.419689)
- Buikema, A., et al. 2020, Phys. Rev. D, 102, 062003, doi: [10.1103/PhysRevD.102.062003](https://doi.org/10.1103/PhysRevD.102.062003)
- Cahillane, C., et al. 2017, Phys. Rev. D, 96, 102001, doi: [10.1103/PhysRevD.96.102001](https://doi.org/10.1103/PhysRevD.96.102001)
- Capote, E., et al. 2025, Phys. Rev. D, 111, 062002, doi: [10.1103/PhysRevD.111.062002](https://doi.org/10.1103/PhysRevD.111.062002)
- Caudill, S., Kandhasamy, S., Lazzaro, C., et al. 2021, Mod. Phys. Lett. A, 36, 2130022, doi: [10.1142/S0217732321300226](https://doi.org/10.1142/S0217732321300226)
- Chatterji, S. K. 2005, PhD thesis, Massachusetts Institute of Technology
- Chen, D., Hido, S., Tuyenbayev, D., et al. 2025, arXiv e-prints, arXiv:2504.12657, doi: [10.48550/arXiv.2504.12657](https://doi.org/10.48550/arXiv.2504.12657)
- Chen, H.-Y., Holz, D. E., Miller, J., et al. 2021, Class. Quant. Grav., 38, 055010, doi: [10.1088/1361-6382/abd594](https://doi.org/10.1088/1361-6382/abd594)
- Collaboration, T. L. S., the Virgo Collaboration, & the KAGRA Collaboration. 2025, GW231123: a Binary Black Hole Merger with Total Mass 190-265 M_{\odot} . <https://arxiv.org/abs/2507.08219>
- Cornish, N. J., Littenberg, T. B., Bécsy, B., et al. 2021, Phys. Rev. D, 103, 044006, doi: [10.1103/PhysRevD.103.044006](https://doi.org/10.1103/PhysRevD.103.044006)
- Covas, P., Effler, A., Goetz, E., Meyers, P., et al. 2018, Physical Review D, 97, doi: [10.1103/physrevd.97.082002](https://doi.org/10.1103/physrevd.97.082002)
- Covas, P. B., Effler, A., Goetz, E., et al. 2018, PhRvD, 97, 082002, doi: [10.1103/PhysRevD.97.082002](https://doi.org/10.1103/PhysRevD.97.082002)
- Davis, D., Massinger, T. J., Lundgren, A. P., et al. 2019, Class. Quant. Grav., 36, 055011, doi: [10.1088/1361-6382/ab01c5](https://doi.org/10.1088/1361-6382/ab01c5)
- Davis, D., et al. 2021, Class. Quant. Grav., 38, 135014, doi: [10.1088/1361-6382/abfd85](https://doi.org/10.1088/1361-6382/abfd85)
- Dooley, K. L., et al. 2016, Class. Quant. Grav., 33, 075009, doi: [10.1088/0264-9381/33/7/075009](https://doi.org/10.1088/0264-9381/33/7/075009)
- Driggers, J. C., et al. 2019, Phys. Rev. D, 99, 042001, doi: [10.1103/PhysRevD.99.042001](https://doi.org/10.1103/PhysRevD.99.042001)
- Essick, R., Godwin, P., Hanna, C., Blackburn, L., & Katsavounidis, E. 2020, Machine Learning: Science and Technology, 2, 015004, doi: [10.1088/2632-2153/abab5f](https://doi.org/10.1088/2632-2153/abab5f)
- Essick, R., Mo, G., & Katsavounidis, E. 2021, Phys. Rev. D, 103, 042003, doi: [10.1103/PhysRevD.103.042003](https://doi.org/10.1103/PhysRevD.103.042003)
- Finn, L. S., & Chernoff, D. F. 1993, Phys. Rev. D, 47, 2198, doi: [10.1103/PhysRevD.47.2198](https://doi.org/10.1103/PhysRevD.47.2198)
- Ghonge, S., Brandt, J., Sullivan, J. M., et al. 2024, Phys. Rev. D, 110, 122002, doi: [10.1103/PhysRevD.110.122002](https://doi.org/10.1103/PhysRevD.110.122002)
- Glanzer, J., et al. 2023, Class. Quant. Grav., 40, 065004, doi: [10.1088/1361-6382/acb633](https://doi.org/10.1088/1361-6382/acb633)
- Gurav, R., Kelly, I., Goodarzi, P., et al. 2024, doi: [10.1109/BigData62323.2024.10825388](https://doi.org/10.1109/BigData62323.2024.10825388)
- Hourihane, S., Chatziioannou, K., Wijngaarden, M., et al. 2022, Phys. Rev. D, 106, 042006, doi: [10.1103/PhysRevD.106.042006](https://doi.org/10.1103/PhysRevD.106.042006)
- Hunter, J. D. 2007, Comput. Sci. Eng., 9, 90, doi: [10.1109/MCSE.2007.55](https://doi.org/10.1109/MCSE.2007.55)
- Huxford, R., George, R., Trevor, M., Yarbrough, Z., & Godwin, P. 2024. <https://arxiv.org/abs/2412.04638>
- IGWN Computing and Software Working Group. 2025, IGWN Conda Environment, <https://computing.docs.ligo.org/conda/>
- Jia, W., et al. 2024, Science, 385, 1318, doi: [10.1126/science.ado8069](https://doi.org/10.1126/science.ado8069)
- Karki, S., et al. 2016, Rev. Sci. Instrum., 87, 114503, doi: [10.1063/1.4967303](https://doi.org/10.1063/1.4967303)
- Koziol, Q., & Robinson, D. 2018, HDF5. <https://doi.org/10.11578/dc.20180330.1>

- Kwok, J. Y. L., Lo, R. K. L., Weinstein, A. J., & Li, T. G. F. 2022, Phys. Rev. D, 105, 024066, doi: [10.1103/PhysRevD.105.024066](https://doi.org/10.1103/PhysRevD.105.024066)
- LIGO Laboratory. 2025. <https://dcc.ligo.org/LIGO-M1000066/public>
- LIGO Scientific Collaboration and Virgo Collaboration. 2022, Specification of a Common Data Frame Format for Interferometric Gravitational Wave Detectors (v4), Tech. Rep. VIR-067A-08. <https://dcc.ligo.org/LIGO-T970130/public>
- LIGO Scientific Collaboration, Virgo Collaboration and KAGRA Collaboration. 2017, Data release for event GW170817, doi: [10.7935/K5B8566F](https://doi.org/10.7935/K5B8566F)
- . 2021a, O3a Data Release, doi: [10.7935/nfnt-hm34](https://doi.org/10.7935/nfnt-hm34)
- . 2021b, O3b Data Release, doi: [10.7935/pr1e-j706](https://doi.org/10.7935/pr1e-j706)
- . 2022, O3GK Data Release, doi: [10.7935/38s2-7g84](https://doi.org/10.7935/38s2-7g84)
- . 2024, GEO600 Data for FRBs from SGR 1935+2154, doi: [10.7935/j4zw-0376](https://doi.org/10.7935/j4zw-0376)
- . 2025, O4a Data Release, doi: [10.7935/kt51-6n86](https://doi.org/10.7935/kt51-6n86)
- LIGO, Virgo, and KAGRA. 2019. <https://dcc.ligo.org/LIGO-M1900145/public>
- . 2025. <https://dcc.ligo.org/LIGO-T2100313/public>
- Luck, H., et al. 2010, J. Phys. Conf. Ser., 228, 012012, doi: [10.1088/1742-6596/228/1/012012](https://doi.org/10.1088/1742-6596/228/1/012012)
- Macas, R., Pooley, J., Nuttall, L. K., et al. 2022, Phys. Rev. D, 105, 103021, doi: [10.1103/PhysRevD.105.103021](https://doi.org/10.1103/PhysRevD.105.103021)
- Macleod, D. M., Areeda, J. S., Coughlin, S. B., Massinger, T. J., & Urban, A. L. 2021, SoftwareX, 13, 100657, doi: [10.1016/j.softx.2021.100657](https://doi.org/10.1016/j.softx.2021.100657)
- Nguyen, P., Schofield, R. M. S., Effler, A., et al. 2021, Classical and Quantum Gravity, 38, 145001, doi: [10.1088/1361-6382/ac011a](https://doi.org/10.1088/1361-6382/ac011a)
- Nguyen, P., et al. 2021, Class. Quant. Grav., 38, 145001, doi: [10.1088/1361-6382/ac011a](https://doi.org/10.1088/1361-6382/ac011a)
- Nuttall, L., et al. 2015, Class. Quant. Grav., 32, 245005, doi: [10.1088/0264-9381/32/24/245005](https://doi.org/10.1088/0264-9381/32/24/245005)
- Nuttall, L. K. 2018, Phil. Trans. Roy. Soc. Lond. A, 376, 20170286, doi: [10.1098/rsta.2017.0286](https://doi.org/10.1098/rsta.2017.0286)
- Nyquist, H. 1924, Bell System Technical Journal, 3, 324, doi: [10.1002/j.1538-7305.1924.tb01361.x](https://doi.org/10.1002/j.1538-7305.1924.tb01361.x)
- Olsen, S., Venumadhav, T., Mushkin, J., et al. 2022, Phys. Rev. D, 106, 043009, doi: [10.1103/PhysRevD.106.043009](https://doi.org/10.1103/PhysRevD.106.043009)
- Pankow, C., et al. 2018, Phys. Rev. D, 98, 084016, doi: [10.1103/PhysRevD.98.084016](https://doi.org/10.1103/PhysRevD.98.084016)
- Rollins, J. G. 2016, Rev. Sci. Instrum., 87, 094502, doi: [10.1063/1.4961665](https://doi.org/10.1063/1.4961665)
- Smith, S. W. 1999, The Scientist and Engineer's Guide to Digital Signal Processing (California Technical Publishing). www.DSPguide.com
- Soni, S., Austin, C., Effler, A., et al. 2021, Classical and Quantum Gravity, 38, 025016, doi: [10.1088/1361-6382/abc906](https://doi.org/10.1088/1361-6382/abc906)
- Soni, S., Glanzer, J., Effler, A., et al. 2024, Class. Quant. Grav., 41, 135015, doi: [10.1088/1361-6382/ad494a](https://doi.org/10.1088/1361-6382/ad494a)
- Soni, S., et al. 2025, Class. Quant. Grav., 42, 085016, doi: [10.1088/1361-6382/adc4b6](https://doi.org/10.1088/1361-6382/adc4b6)
- Sun, L., et al. 2020, Class. Quant. Grav., 37, 225008, doi: [10.1088/1361-6382/abb14e](https://doi.org/10.1088/1361-6382/abb14e)
- . 2021. <https://arxiv.org/abs/2107.00129>
- Tse, M., et al. 2019, Phys. Rev. Lett., 123, 231107, doi: [10.1103/PhysRevLett.123.231107](https://doi.org/10.1103/PhysRevLett.123.231107)
- Usman, S. A., et al. 2016, Class. Quant. Grav., 33, 215004, doi: [10.1088/0264-9381/33/21/215004](https://doi.org/10.1088/0264-9381/33/21/215004)
- Vajente, G., Huang, Y., Isi, M., et al. 2020, Phys. Rev. D, 101, 042003, doi: [10.1103/PhysRevD.101.042003](https://doi.org/10.1103/PhysRevD.101.042003)
- Vallisneri, M., Kanner, J., Williams, R., Weinstein, A., & Stephens, B. 2015, J. Phys. Conf. Ser., 610, 012021, doi: [10.1088/1742-6596/610/1/012021](https://doi.org/10.1088/1742-6596/610/1/012021)
- Viets, A., & Wade, M. 2021. <https://dcc.ligo.org/LIGO-T2100058/public>
- Viets, A., et al. 2018, Class. Quant. Grav., 35, 095015, doi: [10.1088/1361-6382/aab658](https://doi.org/10.1088/1361-6382/aab658)
- Virtanen, P., et al. 2020, Nature Meth., 17, 261, doi: [10.1038/s41592-019-0686-2](https://doi.org/10.1038/s41592-019-0686-2)
- Wade, M., et al. 2025. <https://arxiv.org/abs/2508.08423>
- Zackay, B., Venumadhav, T., & Zaldarriaga, M. 2023, Application for the release of a set of auxiliary channels from the O3, Tech. Rep. T2300274. <https://dcc.ligo.org/LIGO-T2300274/public>
- Zweizig, J., & Riles, K. 2020, Information on self-gating of $h(t)$ used in O3 continuous-wave and stochastic searches, Tech. Rep. T2000384. <https://dcc.ligo.org/LIGO-T2000384/public>
- Zweizig, Z., Maros, E., Hanks, J., & Areeda, J. 2021. <https://wiki.ligo.org/Computing/NDSCClient/>